Mechanisms of Beat-to-Beat Regulation of Cardiac Pacemaker Cell Function by Ca^{2+} Cycling Dynamics

Yael Yaniv, Michael D. Stern, Edward G. Lakatta, and Victor A. Maltsev*
Laboratory of Cardiovascular Science, Intramural Research Program, National Institute on Aging, National Institutes of Health, Baltimore, Maryland

ABSTRACT Whether intracellular Ca^{2+} cycling dynamics regulate cardiac pacemaker cell function on a beat-to-beat basis remains unknown. Here we show that under physiological conditions, application of low concentrations of caffeine (2–4 mM) to isolated single rabbit sinoatrial node cells acutely reduces their spontaneous action potential cycle length (CL) and increases Ca^{2+} transient amplitude for several cycles. Numerical simulations, using a modified Maltsev-Lakatta coupled-clock model, faithfully reproduced these effects, and also the effects of CL prolongation and dysrhythmic spontaneous beating (produced by cytosolic Ca^{2+} buffering) and an acute CL reduction (produced by flash-induced Ca^{2+} release from a caged Ca^{2+} buffer), which we had reported previously. Three contemporary numerical models (including the original Maltsev-Lakatta model) failed to reproduce the experimental results. In our proposed new model, Ca^{2+} releases acutely change the CL via activation of the Na^{+}/Ca^{2+} exchanger current. Time-dependent CL reductions after flash-induced Ca^{2+} releases (the memory effect) are linked to changes in Ca^{2+} available for pumping into sarcoplasmic reticulum which, in turn, changes the sarcoplasmic reticulum Ca^{2+} load, diastolic Ca^{2+} releases, and Na^{+}/Ca^{2+} exchanger current. These results support the idea that Ca^{2+} regulates CL in cardiac pacemaker cells on a beat-to-beat basis, and suggest a more realistic numerical mechanism of this regulation.

INTRODUCTION

Experimental studies of the last two decades have established that intracellular Ca^{2+} signaling contributes to regulation of normal cardiac pacemaker cell function (1–6). Automaticity of the sinoatrial nodal cell (SANC), the primary cardiac pacemaker cells, has been suggested (7) to be regulated by a system of two clock-like oscillators: the sarcoplasmic reticulum (SR), acting as a Ca^{2+} clock, rhythmically discharges diastolic local Ca^{2+} releases (LCRs) beneath the cell surface membrane; and LCRs activate an inward Na^{+}-Ca^{2+} exchanger current (I_{NCX}) that accelerates diastolic depolarization (DD) and prompts the surface membrane-clock (M clock), an ensemble of sarcolemmal electrogenic molecules, to generate an action potential (AP) (Fig. 1). Because the M clock regulates SANC Ca^{2+} influx and efflux, it also regulates the Ca^{2+} clock, forming a coupled-clock system (8,9). The coupled-clock system hypothesis is continually being rigorously debated (10,11) and experimentally challenged (12). Therefore, in this article we provide additional experimental and numerical validation of the coupled clock pacemaker cell concept.

Specifically, we had previously demonstrated that membrane potential fluctuations resulting from the LCRs impart an exponential phase to the late DD that controls the SANC chronotropic state (13). However, in that study, noise characteristics of the membrane potential and LCRs were compared at a given steady state as averaged values over several beats (rather than in a given beat). Our more recent measurements using a high-speed camera demonstrated that spontaneous, beat-to-beat AP cycle variations are linked to the characteristics of the entire LCR ensemble in any, given cycle (14). The idea of dynamic (beat-to-beat) interactions of the two clocks that ultimately determine the duration of each AP cycle length (CL) has been also validated, in part, by a demonstration that acute flash-induced Ca^{2+} release from an intracellular caged buffer (NP-EGTA) produces acute changes in intracellular Ca^{2+} dynamics, which result in instantaneous changes in the CL (15). However, in that study, before the flash was applied, SANCs were exposed to artificial Ca^{2+} buffering that had substantially prolonged the initial CL beyond physiological range. Therefore, additional studies are required to demonstrate beat-to-beat regulation of CL under physiological conditions. Moreover, specific mechanisms describing how each clock entrains the other remain unknown and require a dedicated numerical investigation. Specifically, it remains unknown, how the membrane Ca^{2+}-dependent molecules are affected by release of Ca^{2+} in a beat-to-beat manner in response to Ca^{2+} perturbation, and how the Ca^{2+}-induced M clock changes entrain the Ca^{2+} clock.

This study tested whether intracellular Ca^{2+} release can regulate the AP firing rate in a beat-to-beat manner at a physiological AP firing rate. To this end, we acutely applied (brief application) low concentrations of caffeine (2–4 mM) onto spontaneously beating SANC, via a picospritzer, to acutely increase open probability of their SR Ca^{2+} release channels (RyR) (Fig. 1). To accurately interpret the experimental results and to gain mechanistic insight into the beat-to-beat Ca^{2+} regulation of CL, we performed a detailed numerical investigation of these effects. Surprisingly, we found that the experimental results cannot be reproduced

Submitted February 6, 2013, and accepted for publication August 15, 2013.
*Correspondence: maltsevvi@grc.nia.nih.gov
Editor: David Piston.

0006-3495/13/10/1551/11 $2.00
http://dx.doi.org/10.1016/j.bpj.2013.08.024

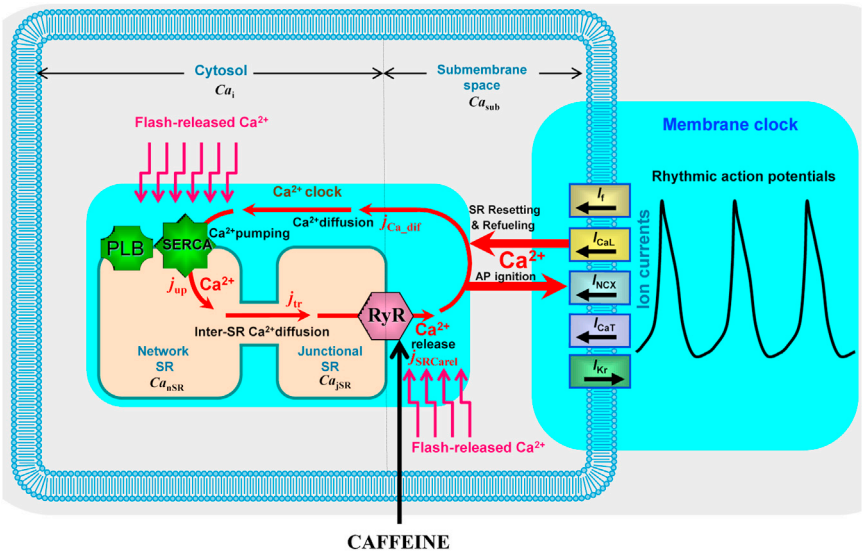

FIGURE 1 Schematic illustrations of the coupled-clock system. In our experimental results and numerical model simulations, the interplay of sarcoplasmic reticulum Ca^{2+} cycling proteins and ion channels in SANC is perturbed by either flash-induced Ca^{2+} release (*zigzag arrows*) or by caffeine-induced Ca^{2+} release (*solid arrow*).

by any existing models of the rabbit SA node cell, such as the model of Kurata et al. (16), the original Maltsev-Lakatta coupled-clock model (17), and its updated version by Severi et al. (18). Our proposed new model (modification of the Maltsev-Lakatta model) functionally reproduced the new experimental data, and provided more realistic numerical mechanisms underlying cardiac pacemaker function.

MATERIALS AND METHODS

Cell preparation

Single SANCs were isolated from New Zealand White rabbit hearts as previously described in Vinogradova et al. (19). The experiment protocols have been approved by the Animal Care and Use Committee of the National Institutes of Health (protocol No. 034LCS2013). The dissociated cells were stored at 4°C and were used within 8 h of isolation.

Confocal imaging of AP-triggered Ca^{2+} transients

SANCs were placed in a laminated chamber (25 μg/mL; Invitrogen, Carlsbad, CA) on an inverted microscope and were loaded with 5 μM Fluo-4AM (Molecular Probes, Eugene, OR) (see below for details), and subsequently superfused with a Tyrode's solution with the following composition: 140 mM NaCl, 5.4 mM KCl, 2 mM $MgCl_2$, 5 mM HEPES, 1.8 mM $CaCl_2$, and 5.5 mM Glucose, titrated to pH 7.4 with NaOH. Ca^{2+} fluorescence was imaged on a LSM510 confocal microscope (Carl Zeiss, Oberkochen, Germany) using a 40×/1.3 N.A. oil immersion lens. Cells were excited with the 488-nm light of an argon laser, and fluorescence emission was collected with a long-pass 505-nm filter. All images were recorded with a scan line (512 × 1 pixels at 14.9 pixel/μm and 2 ms/line) oriented across the cell length, and processed with the software MATLAB (The MathWorks, Natick, MA). All measurements of Ca^{2+} signals were conducted at 35 ± 0.5°C. The CL was measured as the time period between subsequent Ca^{2+} transient peaks. Because each AP induces a Ca^{2+} transient, the AP cycle length and Ca^{2+} transient cycle length are extremely close to each other, as demonstrated by our simultaneous recordings of APs and Ca^{2+} transients (see Fig. S1 in the Supporting Material). In other words, the CL can be accurately measured using recordings of Ca^{2+} transients induced by APs.

Acute caffeine application

We employed a brief rapid application of caffeine onto the cell by pressure-ejection (using a picospritzer) via a nearby pipette. Two types of caffeine experiments were performed in this study. One set of experiments utilized high caffeine concentrations of 10 mM (for 1 s) to induce Ca^{2+} transients to assess the SR Ca^{2+} content. For these experiments, nine SANCs from three rabbits were used. Another set of experiments utilized lower caffeine concentrations of 2–4 mM (for 1 s) to test the instant effect of caffeine on the spontaneous rate and other characteristics of AP-induced Ca^{2+} transients. For these experiments, 11 SANCs from four rabbits were used. To decrease the washout time, the injection glass pipette was mounted so that the caffeine injection flow was oriented in the direction of the chamber solution flow. Further, during caffeine application the bath perfusion rate was increased to 1.5 mL/min to rapidly wash out the caffeine. Our rough estimate using a colored solution and observation of movement of small debris particles near the cells during perfusion indicate that the washout time could be as long as 1 s, giving a total caffeine exposure of ~2 s, as numerically modeled (described below).

Loading SANC with caged Ca^{2+} buffer NP-EGTA and Ca^{2+} indicator Fluo-4

In experiments testing the effect of NP-EGTA on SR Ca^{2+} content, cells were preloaded with both a cell-permeant photolabile chelator of intracellular Ca^{2+} NP-EGTA AM (15 μM, Invitrogen) and a Ca^{2+} indicator Fluo-4 AM (5 μM, Invitrogen) for 25 min at room temperature. In experiments testing the effect of low concentration of caffeine, cells were loaded with 5 μM Fluo-4AM for 20 min at room temperature.

Modifications to the original Maltsev-Lakatta numerical model of SANC

To simulate the effects of an acute change in Ca^{2+} cycling dynamics on CL, we used both the original 2009 Maltsev-Lakatta numerical model of rabbit SANC (17) and its modification. All formulations and parameters of the modified model used in this article are provided in the Supporting Material. In this study, we excluded a nonselective I_{st} current, because this current has properties of I_{NCX} and I_{CaL} and its molecular identity has not been established (see details in Maltsev and Lakatta (20)). I_{Ks} was excluded because of its small expression in rabbit SANC. Finally, the amplitudes of both

inward Na^+ background current (I_{bNa}) and outward Na/K-ATPase current (I_{NaK}) were reduced, as recently suggested by Maltsev and Lakatta (20) and DiFrancesco (22). Note that the density of I_f (the so-called funny current) remained unchanged ($g_{If} = 0.15$ nS/pF). A formal I_f blockade in our proposed new model increases AP cycle length from 339.7 to 379.7 ms, which is an increase of 11.8% (beating rate decreases from 176.6 to 158 beats per minute, i.e., by 10.5%).

Table S1 in the Supporting Material lists all variables and their initial values. The membrane potential, V_m, is described as

$$dV_m/dt = -\left(I_{CaL} + I_{CaT} + I_f + I_{Kr} + I_{to} + I_{sus} + I_{NaK} + I_{NCX} + I_{bCa} + I_{bNa}\right)/C_m. \quad (1)$$

The effects of simulated caffeine- and photo-released Ca^{2+} is mediated via a Ca^{2+}-dependence of the ion currents incorporated in the simulations. In our proposed new model, only two currents are Ca^{2+}-dependent: I_{CaL} (via its Ca^{2+}-dependent inactivation, variable f_{Ca}; see the Supporting Material) and I_{NCX}.

Approximation of caffeine effect on RyR release kinetics

The RyR Ca^{2+} release flux was numerically modeled as previously suggested by Stern et al. (23), further modified by Shannon et al. (24), and used in our modeling of SANC (17) (see the Supporting Material for details):

$$j_{SRCarel} = k_s \times O \times \left(Ca_{jSR} - Ca_{sub}\right), \quad (2)$$

$$k_{CaSR} = MaxSR - (MaxSR - MinSR)/\left(1 + \left(EC_{50\_SR}/Ca_{jSR}\right)^{HSR}\right), \quad (3)$$

$$k_{oSRCa} = k_{oCa}/k_{CaSR}, \quad (4)$$

$$k_{iSRCa} = k_{iCa} \times k_{CaSR}, \quad (5)$$

$$dR/dt = (k_{im} \times RI - k_{iSRCa} \times Ca_{sub} \times R) - \left(k_{oSRCa} \times Ca_{sub}^2 \times R - k_{om} \times O\right), \quad (6)$$

$$dO/dt = \left(k_{oSRCa} \times Ca_{sub}^2 \times R - k_{om} \times O\right) - (k_{iSRCa} \times Ca_{sub} \times O - k_{im} \times I), \quad (7)$$

$$dI/dt = (k_{iSRCa} \times Ca_{sub} \times O - k_{im} \times I) - \left(k_{om} \times I - k_{oSRCa} \times Ca_{sub}^2 \times RI\right), \quad (8)$$

$$dRI/dt = \left(k_{om} \times I - k_{oSRCa} \times Ca_{sub}^2 \times RI\right) - (k_{im} \times RI - k_{iSRCa} \times Ca_{sub} \times R). \quad (9)$$

Porta et al. (25) demonstrated that in planar lipid bilayers, caffeine activation of a single RyR2 channel depends on the free Ca^{2+} level on both sides of the channel (i.e., in our case on both submembrane [Ca^{2+}] and lumenal SR [Ca^{2+}]). Because, as of this writing, it is unknown how RyRs are activated by caffeine in intact SANC, we tested three possibilities of caffeine activation of RyR:

1. Via increasing RyR sensitivity to lumenal SR [Ca^{2+}] (parameter EC_{50_SR} in Eq. 3) from 0.45 to 0.225 mM;
2. Via increasing the rate of transition into open state O from reactivated state R (parameter k_{oCa} in Eq. 4) from 10 to 20 $mM^{-2} \times ms^{-1}$; and
3. A combination of the above two changes.

Numerical estimation of the intracellular NP-EGTA concentration

Our formulations for Ca^{2+} buffering by NP-EGTA in the cytosol (f_{CBi}) and in the subspace (f_{CBsub}) are as follows:

$$df_{CBi}/dt = CB\_on\_rate \times Ca_i \times (1 - f_{CBi}) - CB\_off\_rate \times f_{CBi}, \quad (10)$$

where CB_on_rate is the Ca^{2+} association constant for NP-EGTA, CB_off_rate is the Ca^{2+} dissociation constant for NP-EGTA, and Ca_i is the intracellular Ca^{2+} concentration

$$df_{CBsub}/dt = CB\_on\_rate \times Ca_{sub} \times (1 - f_{CBsub}) - CB\_off\_rate \times f_{CBsub}, \quad (11)$$

where Ca_{sub} is the subspace Ca^{2+} concentration.

Formulations of Ca^{2+} dynamics in cytosolic (Ca_i) and subspace (Ca_{sub}) compartments were complemented by flash release flux j_{PPs} from caged NP-EGTA as follows:

$$dCa_i/dt = \left(j_{Ca\_dif} \times V_{sub} - j_{up} \times V_{nSR}\right)/V_i - (CB\_Conc \times f_{CBi}/dt + CM_{tot} \times df_{CMi}/dt + TC_{tot} \times df_{TC}/dt + TMC_{tot} \times df_{TMC}/dt) + j_{PPs}. \quad (12)$$

$$dCa_{sub}/dt = j_{SRCarel} \times V_{jSR}/V_{sub} - (I_{CaL} + I_{CaT} + I_{bCa} - 2 \times I_{NCX})/(2 \times F \times V_{sub}) - (CB\_Conc \times f_{CBsub}/dt) + j_{Ca\_dif} + CM_{tot} \times df_{CMs}/dt + j_{PPs}. \quad (13)$$

Simulations using other models

We also tested whether the contemporary models of Kurata et al. (16) and Severi et al. (18) would reproduce effects of caffeine- and flash-induced Ca^{2+} release measured experimentally in SA node cells. For this comparison, we performed simulations using the Cellular Open Resource program developed and maintained at Oxford University (http://cor.physiol.ox.ac.uk). Cellular Open Resource can run numerous cell models, including these two models, in the CellML format available at http://www.cellml.org.

Statistical analysis

Data are presented as mean ± SE. A linear mixed-effects model with Dunnett's method to adjust p values was used (26). This model accounts for repeated measurements on the same preparation while allowing testing for differences among different beats. $P < 0.05$ was taken to indicate statistical significance.

RESULTS

Rapid application of caffeine affects the Ca^{2+} transient characteristics and cycle length

Fig. 2 *A* illustrates representative examples of the effect of caffeine to release Ca^{2+} in two SANCs. Caffeine application acutely increased the systolic Ca^{2+} transient amplitude (by 12 ± 4%). The caffeine-caused acute effect

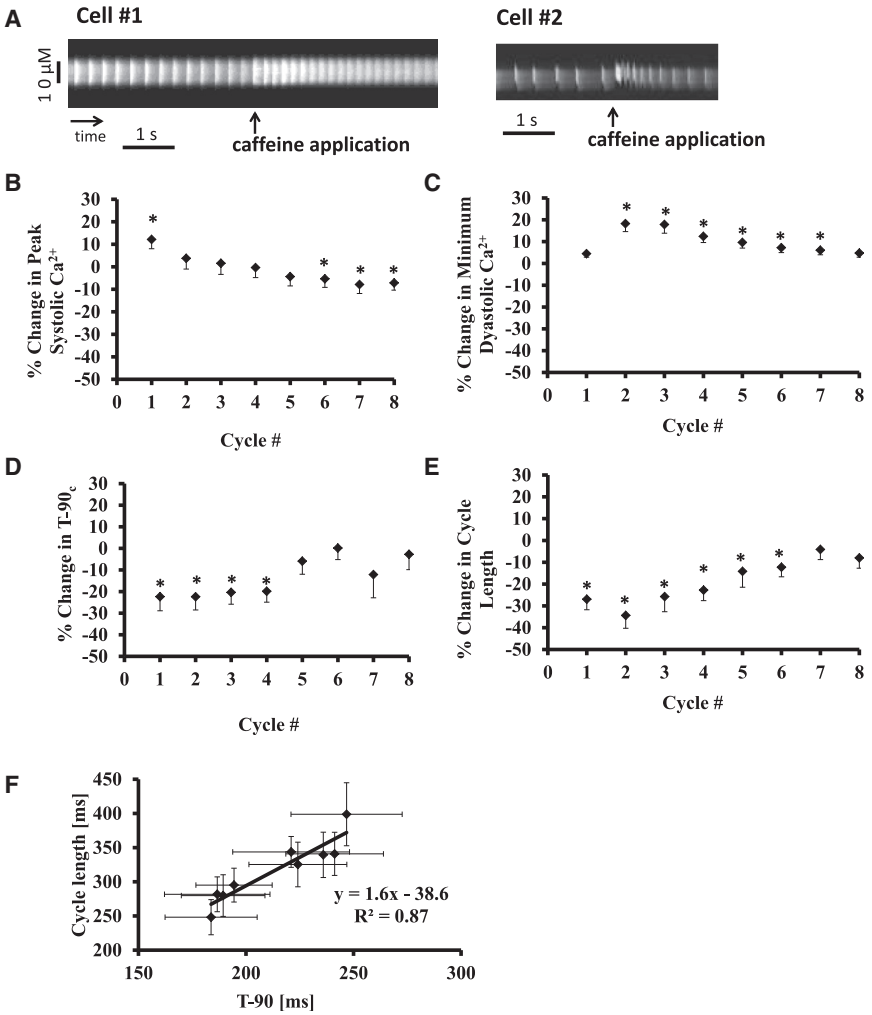

FIGURE 2 Effect of caffeine on the rate of AP-induced Ca^{2+} transients. (*A*) Two representative examples of original recordings of the effect of caffeine on AP-induced Ca^{2+} transients. (*B–E*) Average data obtained in 11 SANcs. An acute application of low concentrations (2–4 mM) of caffeine instantly affects peak systolic Ca^{2+} signal, minimum diastolic Ca^{2+} signal, T-90_c, and cycle length. (*F*) Relationship between cycle length and T-90_c.

ceased over several beats (Fig. 2 *B*). The diastolic [Ca^{2+}] level also acutely increased in response to caffeine by 5 ± 2% on the initial beat, but further increased (by 18 ± 4%) on the following beat (Fig. 2 *C*). The caffeine effect on the diastolic Ca^{2+} level vanished during subsequent cycles (see Table S2). Caffeine reduced the 90% decay time of the AP-induced Ca^{2+} transient (T-90_c) by 22 ± 6% (from 246.7 ± 25.8 to 186.6 ± 24.5 ms) (Fig. 2 *D*). The reduction in Ca^{2+} transient T-90_c on the following beat was similar to that of the initial beat after caffeine application (by 23 ± 6% to 183.7 ± 21.4 ms). Table S2 shows that the caffeine effect on T-90_c vanished after four cycles. Similar reduction trends of the 50% decay time of intracellular Ca^{2+} (T-50_c) were found; however, these were only marginally significant in the two following beats after caffeine application ($P = 0.05$ and $P = 0.0531$). The time-to-peak T_p was not significantly changed by caffeine.

Changes in the AP-induced Ca^{2+} transient cycle length were mirror images of the changes in minimum diastolic Ca^{2+} (Fig. 2 *E*). Before caffeine application, SANCs generated spontaneous rhythmic Ca^{2+} transients with a cycle length of 398.8 ± 46.1 ms ($n = 11$). The initial effect of caffeine application was to markedly reduce the Ca^{2+} transient cycle length by 27 ± 5% (to 281.7 ± 25.5 ms). The maximal reduction in Ca^{2+} transient cycle length (by 34 ± 6%) was achieved in the following beat. Although the caffeine effects subsequently vanished, the CL remained slightly shortened even during washout (Fig. 2 *A*, and see Table S2). This prolonged caffeine effect could be due to its incomplete washout and/or possible CaMKII effects (CaMKII signaling might be activated during the initial caffeine-induced Ca^{2+} increase). Because we could not fully control washout in our experimental system and because our model does not describe CaMKII effects, we did not further study this effect, but focused mainly on several beats upon caffeine application. Note also that the beat-to-beat caffeine-induced changes in the Ca^{2+} transient cycle length are similar to the changes in T-90_c (Fig. 2 *F*) (We have previously demonstrated the crucial importance of T-90_c, reflecting SR Ca^{2+} refilling kinetics, for cardiac pacemaker cell function (27).)

Numerical mechanisms of acute caffeine affect to shorten AP cycle length

We numerically tested three mechanisms of caffeine activation of RyR using different sets of model parameters: by increasing RyR sensitivity to lumenal SR [Ca^{2+}]; by increasing RyR sensitivity to submembrane [Ca^{2+}]; and by employing a combination of the above two changes. The results of our simulations are presented in Fig. 3. All three parameter sets reproduce an experimentally observed increase in diastolic Ca^{2+}, decrease in T-90_c, and initial (first cycle) reduction in cycle length and increase in peak Ca^{2+} transient. However, only the SR Ca^{2+} sensitivity model of caffeine effect (*left columns* in Fig. 3) reproduces the experimentally observed transient change in peak cytosolic Ca^{2+} transients and cycle-length reduction over the next several subsequent cycles. Three existing pacemaker-cell models (Kurata et al. (16), the original Maltsev and Lakatta (17), and Severi et al. (18)) also failed to reproduce the dynamics of the peak cytosolic Ca^{2+} transient measured here (see Fig. S2).

Fig. 4 shows numerical model simulations that provide further mechanistic insights of the caffeine effect to acutely reduce CL in our proposed new model. These model simulations demonstrate that in response to spontaneous caffeine application, LCRs from the SR occur earlier and induce a larger and earlier inward I_{NCX} that, in turn, accelerates the DD, prompting the earlier occurrence of the next AP.

The effect of flash-induced Ca^{2+} release

We have recently demonstrated that NP-EGTA, a caged Ca^{2+} buffer, substantially slows the AP firing rate, and that flash-induced Ca^{2+} release from the buffer instantly reduces CL for several AP cycles (15) (see example of experimental recordings in Fig. 5, *D–F*). In this study we measured caffeine-induced Ca^{2+} transients (as a traditional measure of releasable Ca^{2+} within the SR) before and after NP-EGTA loading into single SANC. Loading of NP-EGTA reduced the caffeine-induced Ca^{2+} release by 15% (Fig. 5, *A–C*). Thus, before flash photolysis, the AP firing rate was slow and dysrhythmic (Fig. 5 *D*), likely due to the abnormally lower SR Ca^{2+} loading and interference of NP-EGTA (as a Ca^{2+} buffer) with Ca^{2+}-dependent processes.

To numerically simulate the effects of NP-EGTA on Ca^{2+} cycling dynamics, it was first necessary to estimate the intracellular NP-EGTA concentration and its effect to perturb SR release Ca^{2+}. The red curve in Fig. 6 *A* shows the relationship between intracellular NP-EGTA concentration and CL predicted by our proposed new model. The CL increased (phase 1) at an NP-EGTA concentration between 1 and 7 mM. The experimentally observed reduction in caffeine-induced Ca^{2+} release (Fig. 5 *C*) is in a good agreement with our modified model prediction of reduction of average network SR [Ca^{2+}] at 8 mM of NP-EGTA (Fig. 6 *B*). At an NP-EGTA concentration between 7 and 9 mM, the CL continued to increase and AP firing became dysrhythmic (phase 2 in Fig. 6 *C*). At still higher NP-EGTA

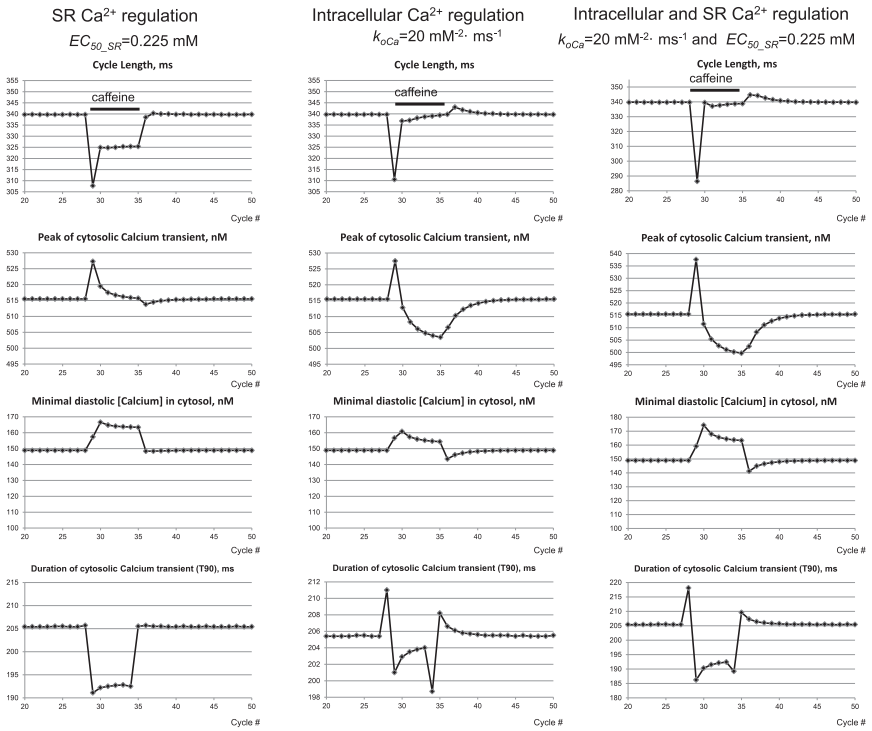

FIGURE 3 Numerical model simulations of SANC responses to acute caffeine application. We explored three different potential mechanisms of RyR activation by caffeine. (*Left column*) Increasing RyR sensitivity to lumenal SR [Ca^{2+}]; (*middle*) increasing RyR sensitivity to submembrane [Ca^{2+}]; and (*right*) a combination of the above two changes. Specific model parameter changes are shown at the top of each column.

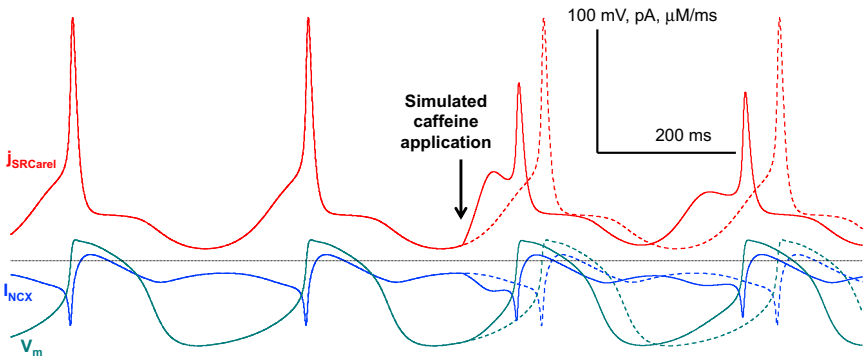

FIGURE 4 Numerical model simulation of the mechanism of the acute caffeine effect. Caffeine acutely increases diastolic Ca^{2+} release ($j_{SRCarel}$), which accelerates diastolic depolarization (V_m trace) via activation of the Na^+/Ca^{2+} exchanger current (I_{NCX}).

concentrations, AP firing ceased (phase 3). Our prior experimental data have shown that in response to NP-EGTA loading, the AP cycle length also increases and becomes dysrhythmic (15). Therefore, to reproduce the present experimental results, we estimated that the buffer concentration in the model should be ~8 mM. This is a reasonable estimate: for example, in the study of Kurata et al. (16), intracellular concentration of EGTA (after cell loading with EGTA-AM) was estimated to be ~10 mM. All three previous numerical models were less sensitive to NP-EGTA and none could reproduce the three phases of the NP-EGTA effect (Fig. 6 *A*, *different colors*).

Surprisingly, the CL in the model of Severi et al. (18) decreased as NP-EGTA concentration increased from 2 to 10 mM (Fig. 6 *A*, *inset*). Our more detailed examination revealed that this model cannot hold Na^+ homeostasis: Na_i drops to 4.6 mM, Ca_{sub} to as low as 39 nM (not shown), and SR Ca^{2+} loading to 0.349 mM (i.e., >3 times) (see Fig. S3), which contradicts the experimental results (Fig. 5, *A–C*). Low intracellular Na^+, in turn, increases diastolic I_{NCX} (from 4.5 to 5.9 pA), which leads to AP rate acceleration (Fig. 6 *A*, *inset*), rather than the substantial rate-slowing observed experimentally, as NP-EGTA concentration increases (Fig. 5 *D*).

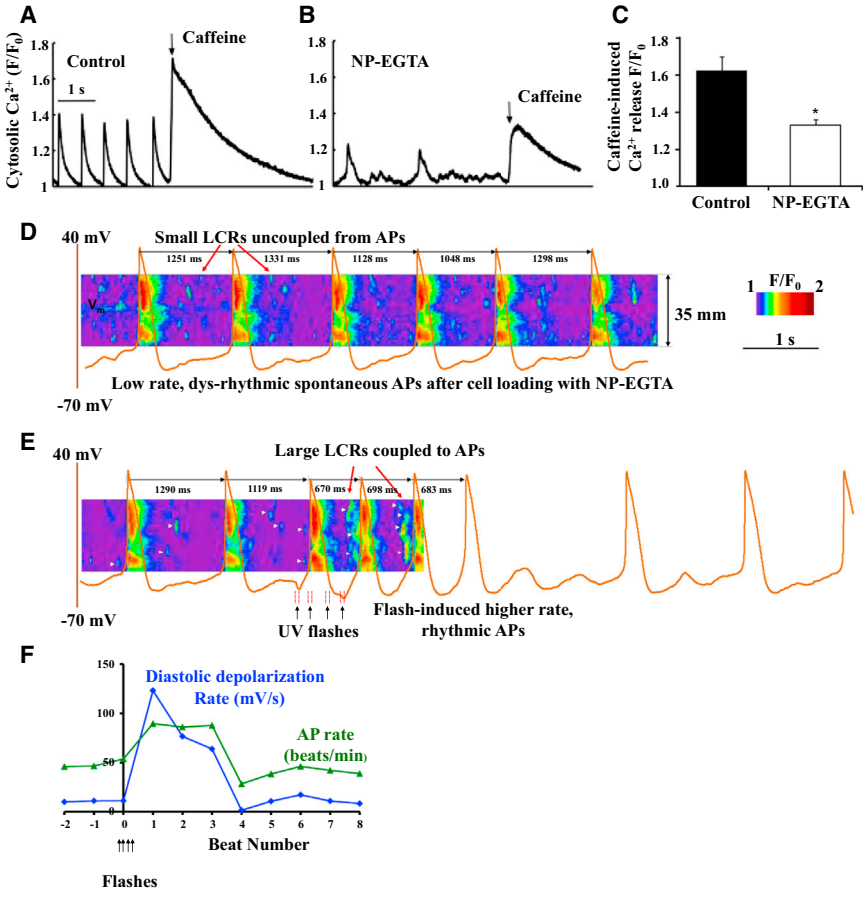

FIGURE 5 Photo-induced release of caged Ca^{2+} acutely reestablishes coupling of the Ca^{2+} clock and the M clock. (*A* and *B*) A representative example of effects of a rapid application of caffeine (indicated by the *arrow*) onto a SANC in control, or after loading SANC with NP-EGTA. (*C*) Average effects of NP-EGTA loading on the amplitude of caffeine-induced cytosolic Ca^{2+} transient ($n = 9$ in control and in the presence of NP-EGTA). (*D–F*) (published previously in Yaniv et al. (15)) The effect of flash-induced Ca^{2+} release on membrane potential and simultaneous Ca^{2+} dynamics in our typical experiment in single rabbit SANC. (*D*) Before the flash, the Ca^{2+} buffer uncoupled LCRs (*line-scan image*) from APs, resulting in a slow, dysrhythmic AP firing rate. (*E*) After the last of four 50-ms UV flashes (*solid arrows*), large, synchronous LCRs emerge (*small white arrows*) and are coupled to the AP occurrence via an acute increase in DD rate, resulting in acute increase in AP firing rate (*F*).

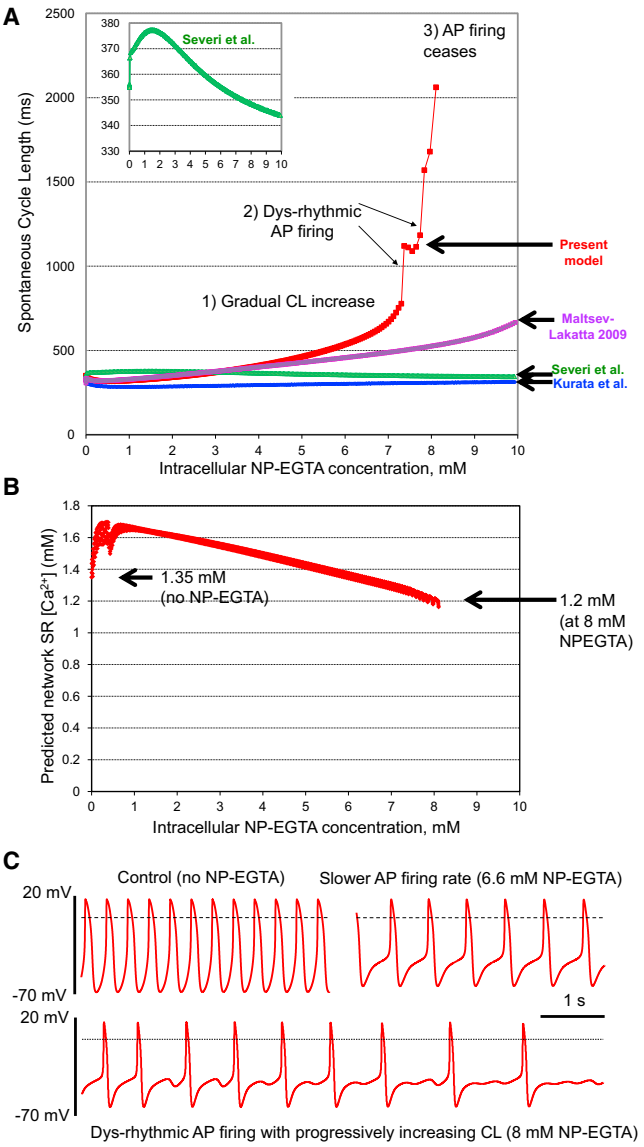

FIGURE 6 Simulations of the steady-state effect of NP-EGTA. (*A*) Predictions of different contemporary models of the change in AP cycle length as a function of intracellular NP-EGTA concentration. Only our proposed new model (i.e., the present model) predicts experimentally observed dynamics of the NP-EGTA effect: gradual CL increase and dysrhythmic AP firing. Although the model of Kurata et al. (16) is almost insensitive to intracellular Ca^{2+} buffering with NP-EGTA, the model of Severi et al. (18) shows CL decrease (rather than the increase observed experimentally) as [NP-EGTA] rises (see details in *inset*). (*B*) Prediction of our proposed new model for network SR Ca^{2+} loading under the same conditions as in panel *A*. (*C*) Representative examples of AP firing, simulated by our proposed new model for different concentrations of intracellular NP-EGTA.

Approximation of photo-released Ca^{2+} rate (j_{PPs})

Upon application of UV flash, a small fraction of caged Ca^{2+} buffer (NP-EGTA) is hydrolyzed into photoproducts (PPs) with much lower affinities for Ca^{2+}. Because the Ca^{2+} unbinding rate for PPs is extremely fast (i.e., ~200,000 faster than that for NP-EGTA: 360 vs. 0.0017 ms^{-1}, as measured by Faas et al. (28)), we did not model the microsecond kinetics of Ca^{2+} release from PPs, but instead approximated the effect of the almost instantly released Ca^{2+} as a constant Ca^{2+} flux with a rate $j_{PPs} = 1$ μM/ms into submembrane space and into cytosol (function of UV pulses intensity). Note that the exact fraction of NP-EGTA turning into PPs by flash remains unknown. Therefore we assigned the dCa_{sub}/dt part via flash-induced Ca^{2+} release (j_{PPs}) to 1 μM/ms to reproduce the moderate effects of flash-induced Ca^{2+} signal increase observed in our control experiments (see the online supplement in Yaniv et al. (15)). For comparison, here we evaluated three benchmarks of dCa_{sub}/dt contributions using Eq. 13 and numerical model predictions for NP-EGTA-loaded SANC spontaneously firing APs:

1. The diastolic Ca^{2+} release flux predicted by the model (at −40 mV) $j_{SRCarel} = 26.6$ μM/ms:

$$(dCa_{sub}/dt)_{diastolic\ release} = j_{SRCarel} \times V_{jSR}/V_{sub} = 26.6 \times 0.12 = 3.192 \mu M/ms.$$

2. The peak systolic Ca^{2+} release predicted by the model $j_{SRCarel} = 75$ μM/ms:

$$(dCa_{sub}/dt)_{systolic\ release} = j_{SRCarel} \times V_{jSR}/V_{sub} = 75 \times 0.12 = 9 \mu M/ms.$$

3. The peak I_{CaL} predicted by the model = 181 pA:

$$(dCa_{sub}/dt)_{via\ peak\ ICaL} = I_{CaL}/(2 \times F \times V_{sub}) = 26.7 \mu M/ms.$$

Thus, our simulated photo-release flux rate $(dCa_{sub}/dt)_{flash} = j_{PPs}$ of 1 μM/ms represents only 31.3 and 11.1% fractions of the diastolic and systolic SR Ca^{2+} release benchmarks, respectively, and only 3.7% of the systolic peak I_{CaL}.

With this relatively small rate of Ca^{2+} release from the buffer (i.e., uncaging), our simulated 4 × 50 ms flashes would require [NP-EGTA] to change by only 200 μM (4 × 50 = 200 ms of 1 μM/ms rate), i.e., by only a small fraction (~2.5%) of the total [NP-EGTA] of ~8 mM (at the time we applied flashes in the model). Therefore, we neglected this change in the [NP-EGTA] (model parameter *CB_Conc*) during the flashes. In turn, the effect of Ca^{2+} binding by PPs was not specifically modeled because the Ca^{2+} binding rate for PPs is the same as for NP-EGTA (*CB_on_rate* = 35 $mM^{-1} \times ms^{-1}$) as measured by Faas et al. (28).

Fig. 7 illustrates the coupled-clock model simulations of the experimentally measured changes in AP firing rate in response to the sequence of four photo-induced Ca^{2+} releases. The model simulations show that changes in intracellular Ca^{2+} can indeed regulate the duration of the same

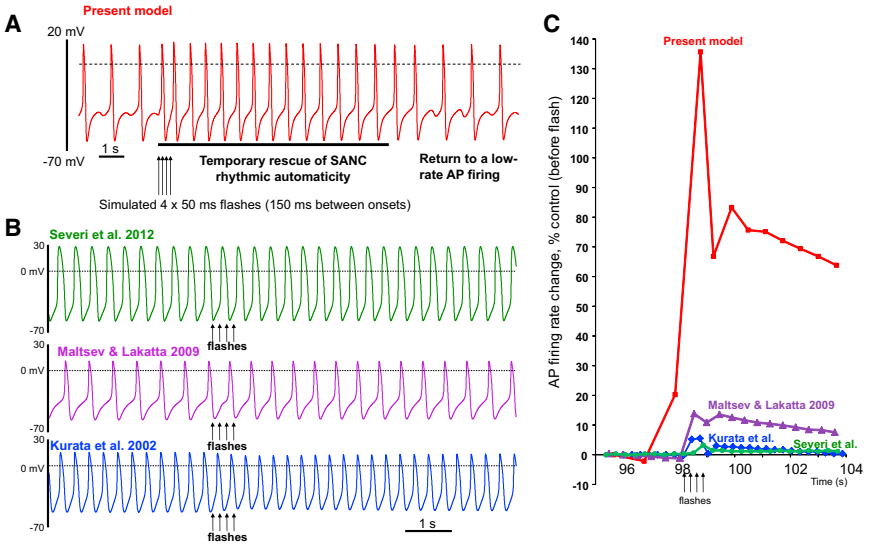

FIGURE 7 Simulations of the effect of flash-induced Ca^{2+} release. (*A*) Similar to experimental results in Fig. 5 *F*, the AP cycle length in our proposed new model simulation becomes temporarily reduced (i.e., rescued) after four 50-ms UV flashes (*solid arrows*). (*B*) In contrast, numerical simulations using different contemporary models fail to predict the AP cycle-length shortening observed experimentally. (*C*) Changes in AP firing rate after four 50-ms UV flashes predicted by the models.

spontaneous cycle in which it was changed, as well as several subsequent spontaneous AP cycles of SANC (the memory effect). Similar to the experimental data (Fig. 5 *E*), the initial effect of the flashes to markedly accelerate DD and acutely reduce cycle length after the termination of the last flash (between simulated beats 3 and 4 in Fig. 7 *A*) occurred at the same beat. After nine rhythmic APs, the effects of the flash waned, due to reestablishment of altered SR Ca^{2+} cycling dynamics by the caged buffer, and the SANC AP firing rate again became slower and dysrhythmic (both in the model and in the experiments; compare Figs. 5 *E* and 7 *A*). Our additional simulations revealed that three previous models had been less sensitive to flash-induced Ca^{2+} and could not reproduce the substantial decrease in the AP cycle length rate after the flashes (Fig. 7, *B* and *C*).

Numerical mechanisms of the effect of photo-released Ca^{2+} on the SANC AP firing rate

In our experiments, four 50-ms flashes were applied experimentally with a time interval of 150 ms between the flashes onsets (*solid arrows* in Fig. 5 *E*). The photo-released Ca^{2+} dramatically affects the DD slope and AP cycle length (Fig. 5 *F*). Simulations using our proposed new model reproduce the marked increase in DD slope after the flash (marked "DD acceleration" in V_m panel in Fig. 8). They also show that with each additional flash-induced Ca^{2+} release the SR load becomes increased and ultimately returns to basal level to ~1.35 mM (Ca_{free_SR} panel in Fig. 8), i.e., the level evaluated under normal conditions, before NP-EGTA (*arrow, no NP-EGTA* in Fig. 6 *B*). Concurrently, diastolic $[Ca^{2+}]_{subspace}$ and I_{NCX} also increase,

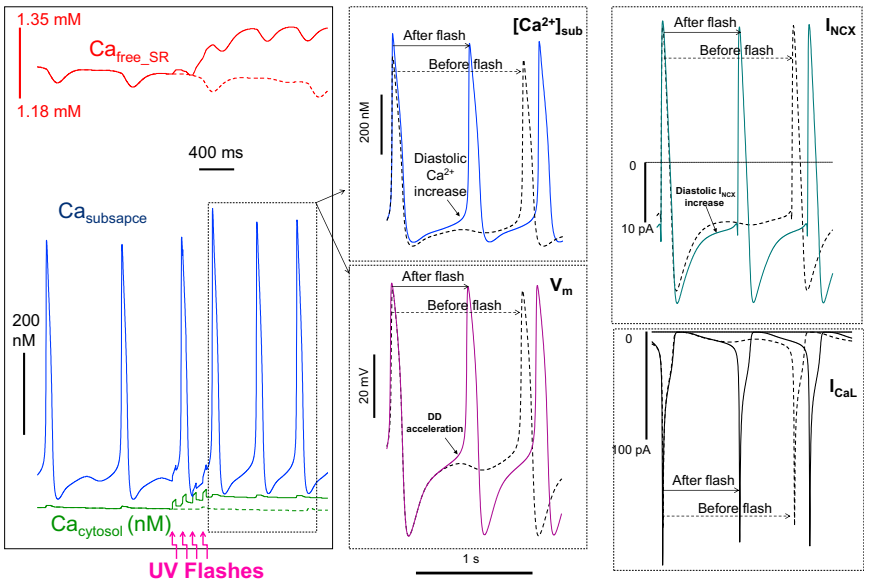

FIGURE 8 Numerical mechanisms that contribute to AP cycle-length shortening caused by photo-released Ca^{2+}. Predicted changes in response to photo-released Ca^{2+}, in the network SR $[Ca^{2+}]$ (Ca_{free_SR}), cytosolic $[Ca^{2+}]$ ($Ca_{cytosol}$), submembrane $[Ca^{2+}]$ ($[Ca^{2+}]_{sub}$), Na^+/Ca^{2+} exchanger current (I_{NCX}), membrane potential (V_m), and L-type Ca^{2+} current (I_{CaL}) are shown. To illustrate the difference, the predicted changes are compared with those in control simulations, i.e., those in which no flashes were applied (*dashed lines*).

driving DD acceleration that normalizes (i.e., rescues) the rate of rhythmic beating (*respective panels* in Fig. 8). This numerical model simulation reproduces the experimental observation of the emergence of large, abundant LCRs after the flash. In other words, the acute, transient, marked reduction in AP cycle length caused by the flash, was likely mediated in our experiments by its effects to markedly increase LCRs, which accelerated the DD via Ca^{2+}-dependent effects on sarcolemmal molecules (such as an increase in the diastolic I_{NCX}).

Our additional model simulations (see Fig. S4) provided an insight into the memory effect observed experimentally (Fig. 5 *E*) and predicted by our proposed new model (Fig. 7 *A*): The flash-induced Ca^{2+} releases nearly-instantaneously elevate both cytosolic and SR Ca^{2+} levels (i.e., the released Ca^{2+} accumulates in the cytosol and within the network SR). Because NCX can extrude only a limited amount of Ca^{2+} each cycle, the intracellular Ca^{2+} levels remain elevated for several pacemaker cycles, which are characterized by a shorter CL. Thus, for the time period of those several cycles, the cell "remembers" the perturbation of its Ca^{2+} balance by flash-induced Ca^{2+} releases.

DISCUSSION

Using two different acute perturbations, i.e., flash-induced Ca^{2+} release and caffeine-induced Ca^{2+} release, our experimental results and numerical model simulations provide strong evidence that changes in intracellular Ca^{2+} dynamics regulate the AP firing rate on a beat-to-beat basis. Specifically, we found that changes in intracellular Ca^{2+} within an AP cycle can regulate the duration of that AP cycle length, and this effect of spontaneous AP cycle length shortening can sustain for several cycles.

Numerical mechanisms

Our numerical model simulations reproduce our proposed new experimental results and also predict that the instantaneous effect of Ca^{2+} regulation on SANC automaticity is produced via activation of I_{NCX} (Fig. 8). The memory effect observed experimentally for several subsequent cycles after flash-induced Ca^{2+} release in SANC, is accomplished in the model simulation via a change in SR Ca^{2+} pumping (see Fig. S4) to regulate SR Ca^{2+} loading, diastolic Ca^{2+} release, and diastolic I_{NCX}.

A brief application of caffeine substantially and acutely decreases the AP cycle length. Caffeine increases the open probability of RyR, and therefore more Ca^{2+} is released by the SR. In ventricular myocytes a low concentration of caffeine increases the frequency and decreases the amplitude of spontaneous Ca^{2+} release (29). In SANC, application of caffeine produced a transient increase in the amplitude of the systolic Ca^{2+} transient, and on the following beats the amplitude of the systolic Ca^{2+} transient decreased (see Table S2), i.e., similar to ventricular myocytes (29). However, in SANC the increase in diastolic $[Ca^{2+}]$ on the following beats is sustained, effecting a reduction of AP cycle length for several beats via activation of diastolic I_{NCX}. We compared three different numerical models of caffeine activation of RyR (Fig. 3) and discovered that the modified model that increases the sensitivity of RyR activation by lumenal SR Ca^{2+} faithfully reproduces all changes in parameters of AP-induced Ca^{2+} transients measured experimentally. Therefore, similar to ventricular myocytes (25) and HEK-293 cells expressing RyR2 (30), a low concentration of caffeine likely affects the sensitivity of RyR activation by lumenal SR Ca^{2+}. Because our experiments were performed under in vitro conditions in single cells, rather than in bilayers, permeabilized cells, or noncardiac HEK cells, we provide, for the first time to our knowledge, insights for the caffeine effect in intact cardiac cells.

Both caffeine- and flash-induced Ca^{2+} release accelerated the decay kinetics of cytosolic Ca^{2+} transient (assessed here as T-90_c). Moreover, the increase in diastolic Ca^{2+} is correlated with the decrease in T-90_c (Fig. 2 *F*). It has been shown previously that T-90_c is highly correlated with the rate of SR Ca^{2+} refilling (27), which critically depends on SR pumping rate and Ca^{2+} available for pumping. Accelerated SR Ca^{2+} refilling, in turn, causes earlier and stronger diastolic Ca^{2+} releases and its attendant I_{NCX}. Therefore, caffeine and flashed-induced Ca^{2+} release accelerate the pacemaker cell rate partially via acceleration of SR Ca^{2+} pumping kinetics, which affects SR Ca^{2+} loading.

Shortcomings of the contemporary pacemaker cell models

An important finding of the study is that existing advanced models of rabbit SA node cell, including Kurata et al. (16), the original Maltsev-Lakatta model (17), and its recent update by Severi et al. (18), failed to reproduce the long-term effect of Ca^{2+} buffering by NP-EGTA and the effects of the acute perturbations of Ca^{2+} dynamics (Figs. 6 and 7, and see Fig. S2). Although the model of Kurata et al. failed mainly because it does not feature a Ca^{2+} clock (i.e., spontaneous diastolic Ca^{2+} release), the two other models are coupled-clock types, and were expected to generate an adequate response. Their surprising failure indicates that these models did not describe important cardiac pacemaker mechanisms. What is the difference between these models and our proposed new model that reproduced the experimental results with critical perturbations of the system? In accord with the ideas of DiFrancesco (22) about the size of currents required for pacemaking and our detailed parametric sensitivity analysis (20), we excluded I_{st} and substantially reduced I_{bNa}. Note that Severi et al. (18) excluded these two currents completely. Compared to the model of Severi et al. (18), however, our proposed

new model keeps Na_i constant at 10 mM. Thus, these comparisons and our additional model simulations (see Fig. S3) can be interpreted to indicate that

1. Na^+ homeostasis is likely more stable in reality than that described by Severi et al. (18); and
2. Additional experimental and numerical model studies are required to clarify Na^+ regulation mechanisms in SANC.

Inadequate Na^+ regulation (homeostasis) in contemporary models may also explain, in part, a recent paradoxical conclusion that I_f harms the robustness of the pacemaker cell system (31).

Study limitations: local Ca^{2+} control and plurality of caffeine targets

Although our simulations favor the idea of caffeine affecting lumenal sensitivity of RyR activation, this result should be treated with some caution, because our model belongs to common-pool models and does not describe local Ca^{2+} regulation. Future modeling of local Ca^{2+} signaling in SANC will clarify this issue.

That caffeine targets molecules other than RyR, needs to be considered when delineating the boundaries of our interpretation of caffeine experiments. Caffeine can act as a phosphodiesterase inhibitor, and therefore it may increase PKA/cAMP that might contribute to the experimentally observed effect on AP firing rate (32). The kinetics of the phosphodiesterase inhibition by caffeine and kinetics of its effect on the downstream targets remain, however, unknown,

I_K in the rabbit SAN consists mainly of I_{Kr} and not I_{Ks} (33). However, the contribution of I_{Ks} to the spontaneous AP firing rate substantially increases during β-adrenergic stimulation (34). Because the macromolecular complex producing I_{Ks} may contain phosphodiesterase (35), inhibition of phosphodiesterase by caffeine can also increase I_{Ks}. However, under basal conditions (as in our study), the role of I_{Ks} in response to caffeine is likely insignificant.

It was shown in smooth muscle of the oviduct that its long exposure (of ~30 s) to caffeine (in the concentration range used in this study) activates the K_{ATP} channel (36). In addition, a K_{ATP} channel opener slows the pacemaker activity of SANC (37). However, in our experiments, spritzing a low concentration of caffeine decreased the CL rather than increased it. Therefore, the opening of K_{ATP} channels is not a major target of caffeine in our conditions. However, higher concentrations of caffeine eliminate the spontaneous AP firing (Fig. 5). Specifically, we previously found that a decrease in spontaneous AP firing is associated with a reduction in cellular ATP (38). Because K_{ATP} channels become open in response to a decrease in intracellular ATP, only a high concentration of caffeine or long-time exposure to caffeine may open K_{ATP} channels in SANC, similar to smooth muscle of the oviduct.

Finally, it has been shown that a long exposure to caffeine, at similar concentrations that were used here, enhances the L-type current and I_f amplitude (39). However, how quickly these channels become affected by caffeine remains unknown. Future experiments are needed to identify additional plausible targets of caffeine.

SUMMARY

Our results support the coupled-clock hypothesis of cardiac pacemaker cell function, i.e., SANC under normal physiological conditions operates as a result of mutual entrainment of an SR-based intracellular Ca^{2+} oscillator (Ca^{2+} clock) and a cell-membrane-based voltage oscillator (M clock) that interact with each other on a beat-to-beat basis. We show that this mutual entrainment is indeed very rapid (actually almost instantaneous) and that the Ca^{2+} clock, generating diastolic Ca^{2+} release, regulates the M clock on a beat-to-beat basis. This quick effect (and clock entrainment) is explained by the coupling of Ca^{2+} signals to the M clock via NCX, an ion exchanger that generates an inward current almost instantly regulated by Na^+/Ca^{2+} gradients during the DD. Our proposed new model simulation of the SR memory effect, in turn, suggests that the diastolic SR Ca^{2+} release depends not only on I_{CaL}-mediated Ca^{2+} influx of the prior cycle, but likely of several (four to nine) prior cycles, and this is an important factor that confers robustness the coupled-clock system. Because our proposed new numerical model (which has constant Na^+) uniquely reproduces the experimental data, whereas other contemporary models (which featured Na^+ dynamics) failed to reproduce the data, our newly gained knowledge about Na^+ homeostasis in SANC is likely incomplete and requires additional experimental studies and numerical modeling approaches.

SUPPORTING MATERIAL

Four figures, two tables and Numerical Model Details are available at http://www.biophysj.org/biophysj/supplemental/S0006-3495(13)00971-5.

The work was supported by the Intramural Research Program of the National Institute on Aging, National Institutes of Health.

REFERENCES

1. Rubenstein, D. S., and S. L. Lipsius. 1989. Mechanisms of automaticity in subsidiary pacemakers from cat right atrium. *Circ. Res.* 64:648–657.
2. Hüser, J., L. A. Blatter, and S. L. Lipsius. 2000. Intracellular Ca^{2+} release contributes to automaticity in cat atrial pacemaker cells. *J. Physiol.* 524:415–422.
3. Rigg, L., B. M. Heath, …, D. A. Terrar. 2000. Localization and functional significance of ryanodine receptors during β-adrenoceptor stimulation in the guinea-pig sino-atrial node. *Cardiovasc. Res.* 48:254–264.
4. Li, J., J. Qu, and R. D. Nathan. 1997. Ionic basis of ryanodine's negative chronotropic effect on pacemaker cells isolated from the sinoatrial node. *Am. J. Physiol.* 273:H2481–H2489.

5. Ju, Y. K., and D. G. Allen. 1998. Intracellular calcium and Na^+-Ca^{2+} exchange current in isolated toad pacemaker cells. *J. Physiol.* 508:153–166.
6. Bogdanov, K. Y., T. M. Vinogradova, and E. G. Lakatta. 2001. Sinoatrial nodal cell ryanodine receptor and Na^+-Ca^{2+} exchanger: molecular partners in pacemaker regulation. *Circ. Res.* 88:1254–1258.
7. Maltsev, V. A., T. M. Vinogradova, and E. G. Lakatta. 2006. The emergence of a general theory of the initiation and strength of the heartbeat. *J. Pharmacol. Sci.* 100:338–369.
8. Lakatta, E. G., V. A. Maltsev, and T. M. Vinogradova. 2010. A coupled system of intracellular Ca^{2+} clocks and surface membrane voltage clocks controls the timekeeping mechanism of the heart's pacemaker. *Circ. Res.* 106:659–673.
9. Yaniv, Y., S. Sirenko, …, E. G. Lakatta. 2013. New evidence for coupled clock regulation of the normal automaticity of sinoatrial nodal pacemaker cells: bradycardic effects of ivabradine are linked to suppression of intracellular Ca^{2+} cycling. *J. Mol. Cell. Cardiol.* 62:80–89.
10. Noble, D., P. J. Noble, and M. Fink. 2010. Competing oscillators in cardiac pacemaking: historical background. *Circ. Res.* 106:1791–1797.
11. DiFrancesco, D., and D. Noble. 2012. The funny current has a major pacemaking role in the sinus node. *Heart Rhythm.* 9:299–301.
12. Himeno, Y., F. Toyoda, …, A. Noma. 2011. Minor contribution of cytosolic Ca^{2+} transients to the pacemaker rhythm in guinea pig sinoatrial node cells. *Am. J. Physiol. Heart Circ. Physiol.* 300:H251–H261.
13. Bogdanov, K. Y., V. A. Maltsev, …, E. G. Lakatta. 2006. Membrane potential fluctuations resulting from submembrane Ca^{2+} releases in rabbit sinoatrial nodal cells impart an exponential phase to the late diastolic depolarization that controls their chronotropic state. *Circ. Res.* 99:979–987.
14. Monfredi, O., L. A. Maltseva, …, V. A. Maltsev. 2013. Beat-to-beat variation in periodicity of local calcium releases contributes to intrinsic variations of spontaneous cycle length in isolated single sinoatrial node cells. *PLoS ONE.* 8:e67247.
15. Yaniv, Y., V. A. Maltsev, …, E. G. Lakatta. 2011. Beat-to-beat Ca^{2+}-dependent regulation of sinoatrial nodal pacemaker cell rate and rhythm. *J. Mol. Cell. Cardiol.* 51:902–905.
16. Kurata, Y., I. Hisatome, …, T. Shibamoto. 2002. Dynamical description of sinoatrial node pacemaking: improved mathematical model for primary pacemaker cell. *Am. J. Physiol. Heart Circ. Physiol.* 283:H2074–H2101.
17. Maltsev, V. A., and E. G. Lakatta. 2009. Synergism of coupled subsarcolemmal Ca^{2+} clocks and sarcolemmal voltage clocks confers robust and flexible pacemaker function in a novel pacemaker cell model. *Am. J. Physiol. Heart Circ. Physiol.* 296:H594–H615.
18. Severi, S., M. Fantini, …, D. DiFrancesco. 2012. An updated computational model of rabbit sinoatrial action potential to investigate the mechanisms of heart rate modulation. *J. Physiol.* 590:4483–4499.
19. Vinogradova, T. M., S. Sirenko, …, E. G. Lakatta. 2008. Constitutive phosphodiesterase activity restricts spontaneous beating rate of cardiac pacemaker cells by suppressing local Ca^{2+} releases. *Circ. Res.* 102:761–769.
20. Maltsev, V. A., and E. G. Lakatta. 2013. Numerical models based on a minimal set of sarcolemmal electrogenic proteins and an intracellular Ca^{2+} clock generate robust, flexible, and energy-efficient cardiac pacemaking. *J. Mol. Cell. Cardiol.* 59:181–195.
21. Reference deleted in proof.
22. DiFrancesco, D. 2010. Considerations on the size of currents required for pacemaking. *J. Mol. Cell. Cardiol.* 48:802–803.
23. Stern, M. D., L. S. Song, …, E. Ríos. 1999. Local control models of cardiac excitation-contraction coupling. A possible role for allosteric interactions between ryanodine receptors. *J. Gen. Physiol.* 113:469–489.
24. Shannon, T. R., F. Wang, …, D. M. Bers. 2004. A mathematical treatment of integrated Ca dynamics within the ventricular myocyte. *Biophys. J.* 87:3351–3371.
25. Porta, M., A. V. Zima, …, M. Fill. 2011. Single ryanodine receptor channel basis of caffeine's action on Ca^{2+} sparks. *Biophys. J.* 100:931–938.
26. Dunnett, C. W., and A. C. Tamhane. 1992. Comparisons between a new drug and active and placebo controls in an efficacy clinical trial. *Stat. Med.* 11:1057–1063.
27. Vinogradova, T. M., D. X. Brochet, …, E. G. Lakatta. 2010. Sarcoplasmic reticulum Ca^{2+} pumping kinetics regulates timing of local Ca^{2+} releases and spontaneous beating rate of rabbit sinoatrial node pacemaker cells. *Circ. Res.* 107:767–775.
28. Faas, G. C., K. Karacs, …, I. Mody. 2005. Kinetic properties of DM-nitrophen binding to calcium and magnesium. *Biophys. J.* 88:4421–4433.
29. Trafford, A. W., G. C. Sibbring, …, D. A. Eisner. 2000. The effects of low concentrations of caffeine on spontaneous Ca release in isolated rat ventricular myocytes. *Cell Calcium.* 28:269–276.
30. Kong, H., P. P. Jones, …, S. R. Chen. 2008. Caffeine induces Ca^{2+} release by reducing the threshold for luminal Ca^{2+} activation of the ryanodine receptor. *Biochem. J.* 414:441–452.
31. Kurata, Y., I. Hisatome, …, T. Shibamoto. 2013. Effect of hyperpolarization-activated current I_f on robustness of sinoatrial node pacemaking: theoretical study on influence of intracellular Na^+ concentration. *Am. J. Physiol. Heart Circ. Physiol.* 304:H1337–H1351.
32. Butcher, R. W., and E. W. Sutherland. 1962. Adenosine 3′,5′-phosphate in biological materials. I. Purification and properties of cyclic 3′,5′-nucleotide phosphodiesterase and use of this enzyme to characterize adenosine 3′,5′-phosphate in human urine. *J. Biol. Chem.* 237:1244–1250.
33. Ono, K., and H. Ito. 1995. Role of rapidly activating delayed rectifier K^+ current in sinoatrial node pacemaker activity. *Am. J. Physiol.* 269:H453–H462.
34. Lei, M., P. J. Cooper, …, P. Kohl. 2002. Role of the 293b-sensitive, slowly activating delayed rectifier potassium current, I_{Ks}, in pacemaker activity of rabbit isolated sino-atrial node cells. *Cardiovasc. Res.* 53:68–79.
35. Terrenoire, C., M. D. Houslay, …, R. S. Kass. 2009. The cardiac I_{Ks} potassium channel macromolecular complex includes the phosphodiesterase PDE4D3. *J. Biol. Chem.* 284:9140–9146.
36. Dixon, R., S. Hwang, …, S. Ward. 2011. Inhibitory effect of caffeine on pacemaker activity in the oviduct is mediated by cAMP-regulated conductances. *Br. J. Pharmacol.* 163:745–754.
37. Han, X., P. E. Light, …, R. J. French. 1996. Identification and properties of an ATP-sensitive K^+ current in rabbit sino-atrial node pacemaker cells. *J. Physiol.* 490:337–350.
38. Yaniv, Y., M. Juhaszova, …, E. G. Lakatta. 2011. Ca^{2+}-regulated-cAMP/PKA signaling in cardiac pacemaker cells links ATP supply to demand. *J. Mol. Cell. Cardiol.* 51:740–748.
39. Satoh, H. 1993. Caffeine depression of spontaneous activity in rabbit sino-atrial node cells. *Gen. Pharmacol.* 24:555–563.